A&A 400, 31–40 (2003)
DOI: 10.1051/0004-6361:20021768

Astronomy & Astrophysics

SPECTRAL: A new evolutionary synthesis code. Application to the irregular Galaxy NGC 1560

G. A. Vázquez⋆, L. Carigi, and J. J. González

Instituto de Astronomía, Universidad Nacional Autónoma de México, A.P. 70-264, D.F. 04510, México
e-mail: carigi@astroscu.unam.mx, jesus@astroscu.unam.mx

Received 23 January 2002 / Accepted 14 November 2002

Abstract. We have developed a new evolutionary synthesis code, which incorporates the output from chemical evolution models. We compare results of this new code with other published codes, and we apply it to the irregular galaxy NGC 1560 using sophisticated chemical evolution models. The code makes important contributions in two areas: a) the generation of synthetic populations with time-dependent star formation rates and stellar populations of different metallicities; b) the extension of the set of stellar tracks from the Geneva group by adding the AGB phases for $m_i/M_\odot \geq 0.8$, as well as the low mass stars. Our code predicts spectra, broad band colors, and Lick indices by using a spectral library, covering a more complete grid of stellar parameters than previous models. The application of the code to the galaxy NGC 1560 constrains the star formation age of its stellar population at around 10.0 Gyr.

Key words. galaxies: evolution – galaxies: stellar content – galaxies: individual: NGC 1560

1. Introduction

The study of the evolutionary history of galaxies includes three important issues: *spectral*, *dynamical*, and *chemical evolution*. Since all these aspects are difficult to include simultaneously in simple galaxy evolution models, studies tend to focus mostly on one of them. Although several efforts to build complete spectro-chemical evolution models have been made (e.g. Tinsley 1972; Arimoto & Yoshii 1986; Einsel et al. 1995; Vazdekis 1996; Moeller et al. 1997; Lindner et al. 1999 among many), it has been difficult to incorporate the new releases of stellar models (stellar structure, evolution, yields, and atmospheres) in to complex galaxy evolution codes. As a result, the spectro-chemical evolution of galaxies has been studied under two complementary but yet limited approaches. While detailed chemical evolution models (e.g. Carigi et al. 1999), constrained mostly from observations of HII regions, represent the independent input for complete spectro-chemical evolution, spectral evolution codes mostly assume simple star formation and chemical enrichment histories. It is therefore very desirable to develop spectro-chemical evolution codes that, tuned and constrained by detailed observations of the interstellar medium in local galaxies, can also be applied with more confidence to high-redshift systems.

The new code (SPECTRAL) presented here makes two important contributions to evolutionary synthesis models: the consideration of a more complete set of evolutionary tracks from the Geneva group, adding tracks to very low stellar masses (Chabrier & Baraffe 1997), and the construction of synthetic populations following a detailed chemical evolution model, in order to derive the spectral properties for systems with a previously modeled enrichment history.

In this paper we initially use simple star formation scenarios to test the new evolutionary synthesis code, and then we proceed to more complete chemical evolution models to constrain the age of the stellar population in the irregular galaxy NGC 1560.

In Sect. 2 we illustrate how the tracks are assembled and describe the spectral library used in the code. In Sect. 3, we describe the process followed to build the evolutionary synthesis code, and the transformation to the observational variables. In Sect. 4, SPECTRAL is tested and compared with others codes commonly used in the field, and we present a first application by predicting spectral properties of the irregular galaxy NGC 1560. Finally, we discuss our conclusions.

2. Stellar tracks

We have incorporated all the tracks from the Geneva group: Schaller et al. (1992, I), Schaerer et al. (1993a, II), Charbonnel et al. (1993, III), Schaerer et al. (1993b, IV), Meynet et al. (1994, V), Charbonnel et al. (1996, VI), Mowlavi et al. (1998, VII) and Charbonnel et al. (1999, VIII) (Lyon group). We combined the Geneva tracks with tracks from Chabrier & Baraffe (1997, CB) for stars with very low mass in order to assemble a complete dual grid of evolutionary tracks for the spectral code (normal and high mass-loss rates) as shown in Table 1. The evolutionary stellar phases considered are main sequence (MS), sub-giant (SG), red giant branch (RGB), zero age horizontal branch (ZAHB) and early asymptotic giant branch (EAGB). The tracks from CB have four evolutionary points

Send offprint requests to: G. A. Vázquez,
e-mail: vazquez@stsci.edu
⋆ At the Space Telescope Science Institute.

Table 1. Ingredients of the selected tracks.

Tracks Group	Phases	Points	Low Mass	High Mass	$Z/Z_\odot$	$\dot{M} \propto$
I, II	M, R,	51	0.8	120	0.05, 0.2	$Z^{0.5}$
III, IV	H[1],				0.4, 1.0	
	E[1]				2.0	
V	M, R,	51	12	120	0.05, 0.2	$5Z^{0.5}$
					0.4, 1.0	
					2.0	
VI	M, R,	54	0.8	1.7	0.05, 1.0	$Z^{0.5}$
	H,					
	E					
VII	M, R,	51	0.8	60	5.0	$Z^{0.5}$
	H[1],					
	E[1]					
VIII	M, R,	51	0.4	1.0	0.05, 1.0	$Z^{0.5}$
CB	P, M,	4	0.075	0.8	0.01, 0.03	0.0
					0.05, 0.1	
					0.3, 1.0	

[1] Only for stars $m_i/M_\odot > 1.7$.
P = Pre-Main Sequence, M = Main Sequence, R = Red Giant Branch, H = Zero Age Horizontal Branch, and E = Early Asymptotic Giant Branch.

Table 2. Evolutionary point number and phases from Geneva tracks.

$M/M_\odot$	$Z/Z_\odot$						Phase
	0.05	0.2	0.4	1.0	2.0	0.1	
Tracks Groups I, II, III, IV, V & VII							
120-85	51	51	51	51	51	-	E
60	51	51	51	51	51	7(M)	E
40-2	51	51	51	51	51	51	E
1.7-1.0	51	51	51	51	51	51	R
0.9	51	51	51	17(S)	21(S)	51	R
0.8	14(S)	51	51	13(S)	21(S)	51	R
Tracks Group VI							
1.7-0.9	54	-	-	54	-	-	E
0.8	24	-	-	24	-	-	R
Tracks Group VIII							
1.0-0.9	51	-	-	51	-	-	R
0.8	51	-	-	14(S)	-	-	R
0.7	11	-	-	11	-	-	M
0.6	6	-	-	5	-	-	M
0.5	3	-	-	4	-	-	M
0.4	2	-	-	3	-	-	M

M = Main Sequence, S = Sub Giant, R = Red Giant Branch, H = Zero Age Horizontal Branch, and E = Early Asymptotic Giant Branch.

Table 3. Main features of the new set of tracks.

Tracks Group	Phases	Points	Low Mass	High Mass	Metallicities	$\dot{M} \propto$
Geneva + Lyon	P-E[1]	84	0.08	120	Z	$Z^{0.5}$
Geneva + Lyon	P-E[1]	84	0.08	120	Z	$5XZ^{0.5}$

Z = 0.001, 0.004, 0.008, 0.02, 0.04, 0.1.
[1] P-E means Pre-Main Sequence, Main Sequence, Red Giant Branch[2], Zero Age Horizontal Branch[2], Early Asymptotic Giant Branch[2]
[1] Only for stars $m_i/M_\odot > 0.7$.

covering two evolutionary phases, pre-main sequence (PMS), and MS.

All tracks are published in such a way that each evolutionary point on each track has an equivalent evolutionary point on the other tracks, as far as they extend to the same phase. However, the total number of time steps on each track differs. During some epochs, phases are under sampled, or are missing all together, as shown in Table 2. As an example of undersampling, the tracks of group VI cover the mass range of $0.8 \leq m_i/M_\odot \leq 1.7$ with 54 evolutionary points up to EAGB, but the RGB is sampled with just 4 points versus 30 of the same tracks in groups I, II, III, and IV. For high mass stars, all tracks undersample the RGB.

On the other hand, as an example of missing phases, the tracks for 0.8 and 0.9 $M_\odot$ in the group I do not reach the RGB for some metallicities (0.001, 0.02 and 0.04).

Our main goal regarding the tracks was to use the principal phases in groups I, II, III, IV and V and complete the tracks and missing phases using tracks from VI, VII, VIII, and CB.

In order to obtain a consistent grid of points, the first step was to re-sample the stellar phases present in all stellar tracks with the same number of evolutionary points. This re-sampling allows us to follow the same stellar phases over all sets of tracks with the same number of evolutionary points. This is the basis of our evolutionary synthesis code.

The second step was to interpolate and extrapolate the missing phases in mass and sometimes in mass and metallicity (of the same group of tracks).

During the third step, we interpolated and extrapolated the ZAHB and EAGB for low-mass stars ($0.8 \leq m_i/M_\odot \leq 1.7$) in metallicity using the tracks of group VI but preserving the shape of the tracks in the group I. These stellar phases are very important for old stellar populations. Finally, we added three PMS evolutionary points for low-mass stars using the tracks from CB.

The stellar variables interpolated in the tracks were stellar age (t_a [years]), temperature ($T_{\rm eff}$), luminosity $L/L_\odot$, and current mass (m_c $[M/M_\odot]$). The independent variables for each step of the grid were evolutionary point (j), initial mass (m_i), and metallicity (Z). Table 3 shows the main features of the two new grids.

2.1. Resampling stellar phases

We used a linear logarithmic interpolation of the stellar variables, which we found to be best suited for this purpose. Figure 1 shows the behavior of one of the stellar variables

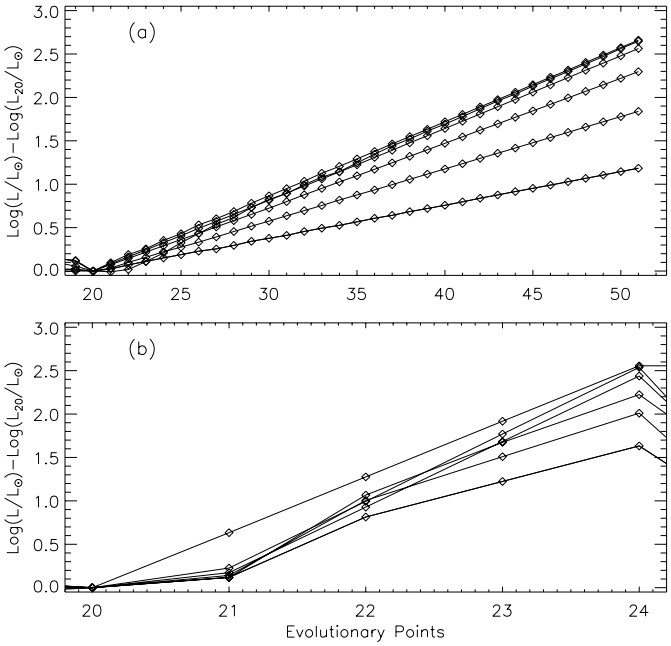

Fig. 1. Luminosity differences as a function of the evolutionary point on RGB in the range of $0.8 \leq m_{\rm i}/M_{\odot} \leq 1.7$ at $Z = 0.001$. **a)** Group I tracks, **b)** group VI tracks.

(luminosity) as a function of the evolutionary point on the RGB to test the efficiency of the linear interpolation to predict the luminosity in the other set of tracks. For the plot, the luminosity is given relative to that of the first point on the RGB ($\log(L/L_{\odot}) - \log(L_{20}/L_{\odot})$) to separate the RGB in each set of tracks and to show the undersampling of this stellar phase in the tracks of group VI.

We have used an IDL code to visualize each interpolation in the tracks, using weights for the linear interpolations defined as:

$$wf_1 = \frac{(f_x - f_{k-1})}{(f_k - f_{k-1})}, \quad wf_0 = 1.0 - wf_1, \tag{1}$$

where f can be one of the independent variables (j, $\log(m_{\rm i})$ or $\log(Z)$), and the k subindices represent adjacent values of this variables. The subindice x can be the new evolutionary point on the track, new mass or new metallicity. New variables (V) were calculated using the equation:

$$V(f) = V(f_{k-1}) \times wf_0 + V(f_k) \times wf_1 \tag{2}$$

where V represents any of the stellar variables ($\log(t_{\rm a})$, $\log(T_{\rm eff})$, $\log(L/L_{\odot})$ and $\log(m_{\rm c})$).

We re-sampled the RGB for all tracks in the range of $1.7 < m_{\rm i}/M_{\odot} \leq 120.0$ to 30 points. In the same way, the tracks of group VI were re-sampled for the same phase to 30 points instead of 4. With this resampling we obtained a final 81 points for all tracks except for those with missing stellar phases.

2.2. Missing phases

We obtained the SG and RGB for masses 0.8 and 0.9 $M_{\odot}$ from groups I, II, III, IV, interpolating in mass or/and metallicity. When we used both, a bilinear interpolation was used, and the new variable was obtained with:

$$\begin{aligned} V(f_a, f_b) \; = \; & V(f_{a_{k-1}}, f_{b_{l-1}}) \times wa_1 \times wb_1 \\ & + V(f_{a_k}, f_{b_{l-1}}) \times wa_0 \times wb_1 \\ & + V(f_{a_k}, f_{b_l}) \times wa_0 \times wb_0 \\ & + V(f_{a_{k-1}}, f_{b_l}) \times wa_1 \times wb_0, \end{aligned} \tag{3}$$

where f_a and f_b are $m_{\rm i}$ and Z, respectively, and the weights (wa and wb) were calculated using the equation (1).

Finally, we interpolated in mass the post RGB evolution in the 0.8 $M_{\odot}$ track from the group VI.

2.3. ZAHB and EAGB for low mass stars

Except for the tracks for masses in the range of $0.8 \leq m_{\rm i}/M_{\odot} \leq 1.7$ in groups I, II, III, IV, which do not have post-RGB evolution, all tracks were re-sampled to 81 points.

To add the ZAHB and EAGB phases for masses in the range of $0.8 \leq m_{\rm i}/M_{\odot} \leq 1.7$ to the tracks in the groups I, II, III, and IV we interpolated and extrapolated in metallicity these phases using tracks from two sets at $Z = 0.001$ and 0.02 of the group VI. We followed the shape of tracks in groups I, II, III, and IV for the RGB and we added the other two phases ZAHB and EAGB in the next form: we have just two points in metallicity (0.001, 0.02), the shape of each stellar variable ($t_{\rm a}$, $m_{\rm c}$, $L/L_{\odot}$, and $T_{\rm eff}$) as a function of metallicity ($F_1(Z)$) of all evolutionary points in group VI is a straight line. In the case of tracks in groups I, II, III, and IV, the function ($F_2(Z)$) is not a straight line.

These two functions $F_1(Z)$ and $F_2(Z)$ were used to transform the tracks in group VI to the shape of tracks in I, II, III, and IV. Then, we defined $Q(Z) = F_1(Z)/F_2(Z)$ as the factor to convert the shape of $F_1(Z)$ into the $F_2(Z)$ shape, or vice versa. For instance, we transform in Fig. 2 the logarithm of luminosity of the evolutionary point 40 (RGB) in tracks I to luminosity of point 40 in group VI as a function of logarithm of metallicity of the track for 1.0 $M_{\odot}$.

We used the last point on RGB of the tracks converted with the previous method as the first point to add the post-RGB evolution to the rest of tracks. Because the logarithm of the stellar variables in the ZAHB and EAGB phases is linear as a function of the evolutionary point, we interpolated in metallicity $\Delta(t_{\rm a})$, $\Delta(m_{\rm c})$, $\Delta(L/L_{\odot})$, $\Delta(T_{\rm eff})$ from the tracks of group VI. With this step we re-sampled all the tracks to 81 points.

The final step to assemble the tracks was to incorporate the stars with very low mass by using the models from CB. An interpolation in metallicity has been done to convert these tracks to the same metallicities as the Geneva tracks using Eqs. (1) and (2). Then, we identified the ZAMS and pre-main sequence points over the four evolutionary points of the CB tracks, and we made the first point on the MS match the first point on the Geneva tracks. This was done because we have used the tracks of group VIII to fix the ZAMS point. For lower mass tracks in CB, point four is the ZAMS, but for higher masses (0.7 and 0.8 $M_{\odot}$) the ZAMS is point 2 or 3. We re-sampled the tracks to have 3 pre-main sequence points and the last point on the MS as the first point of the Geneva tracks. Finally, we have

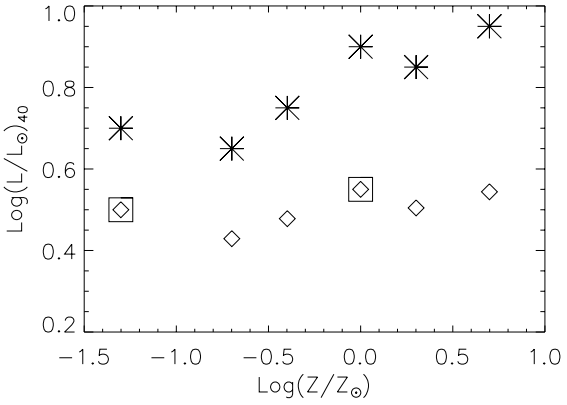

Fig. 2. The luminosity of point 40 in group VI as a function of metallicity of the track for 1.0 $M_{\odot}$. Symbols: squares (evolutionary points from VI group), asterisks (points from I group) and rombes (transformed points).

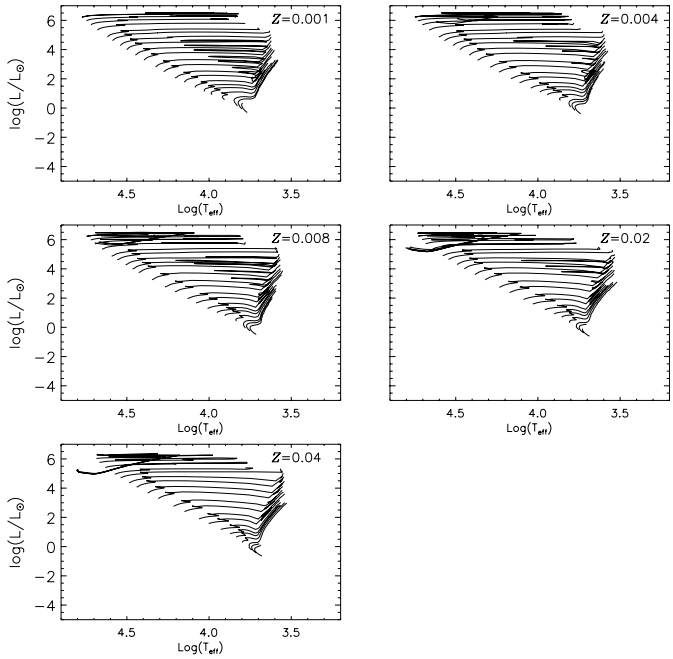

Fig. 3. HR diagrams with tracks I, II, III, IV, and VII from the Geneva group, for masses 0.8–120.0 $M_{\odot}$.

obtained a new set of tracks with 84 equivalent evolutionary points from pre-main sequence up to EAGB.

However, there is no pre-main sequence for higher masses, and for stars in the range of ∼2.0 to 10.0 $M_{\odot}$ there is no AGB. In these cases the ZAMS and the last ZAHB evolutionary points were repeated for numerical reasons.

The tracks in group VII with $Z = 0.1$ were originally incomplete and our method of resampling and completing stellar phases did not succeed. We decided not to use them in this work, but the results can be found in Vázquez (2001).

For comparison we show in Figs. 3 and 4 the original Geneva tracks and the new set of tracks with the new phases, and the new stellar tracks for very low masses with normal mass-loss rates, respectively.

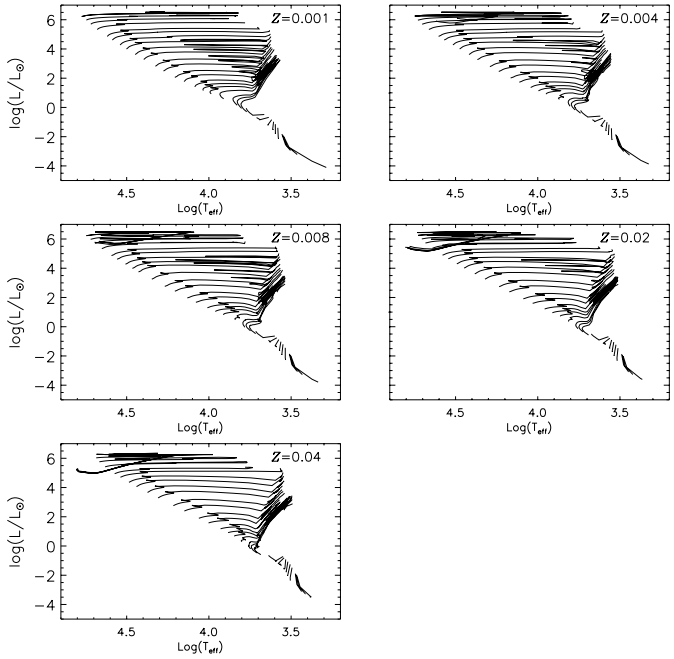

Fig. 4. HR diagrams with sets of tracks for masses 0.08–120.0 $M_{\odot}$.

We can see the pre-main sequence phases included for masses $m_{\rm i}/M_{\odot} \leq 0.7$ in Fig. 4. Finally, we obtained two homogeneous grids to interpolate the stellar variables in time, mass, and metallicity: one with normal mass-loss ($\dot{M} \propto Z^{0.5}$) and a second one using tracks from the group V for masses in the range $12.0 \leq m_{\rm i}/M_{\odot} \leq 120.0$ with high mass-loss rates ($\dot{M} \propto 5 \times Z^{0.5}$). The tracks in group V, which describe the evolution of stars with a higher mass-loss rate were treated in the same way as those of normal mass-loss tracks from groups I, II, III, and IV. To obtain a new set of tracks with a higher mass-loss rate, we just added tracks for lower masses than 12.0 $M_{\odot}$ from the new grid with normal mass-loss rates.

3. The evolutionary synthesis code SPECTRAL

3.1. The input and synthetic stellar populations

The evolutionary synthesis code has been developed in such a way that it is possible to use the output of chemical evolution models (e.g. Carigi et al. 1999; Vázquez 2001) as input to the spectral evolution models in terms of the following quantities:

–Duration of star formation, $t_{\rm SFH}$;

–Star Formation Rate, $\Psi(t)$;

–Metallicity of the interstellar gas, $Z(t)$.

The code calculates the number of stars $n(m_{\rm i}, t)$ formed at any step of time $(t - \Delta t,\ t + \Delta t)$ in the interval $m_{\rm l} \leq m_{\rm i}/M_{\odot} \leq m_{\rm h}$ defined as follows:

$$n(m_{\rm i}, t) = \Phi(m_{\rm i})\Psi(t) \quad (4)$$

where $m_{\rm l}$, $m_{\rm h}$ are the lower and upper limits in mass, respectively, and $\Phi(m_{\rm i})$ is the initial mass function.

$Z(t)$ is the metallicity of the gas from which a new stellar population is born. Stars are assumed to form with the metallicity given by the chemical evolution models for the time of their birth.

The stellar population seen at *Age* of 10.0 Gyr, e.g., is the number of stars still alive and formed in every time step over the whole continuous star formation history from $t = 0$ up to $t_{\rm SFH}$ with a given SFR (in this case the oldest stars are on the EAGB). $t_{\rm SFH}$ can be an instant when we model instantaneous burst, but if $t_{\rm SFH} = Age$ (star formation is ongoing), then the result of this process is that most of the stars formed in the first generation have died after 10.0 Gyr, and just the stars with very low mass are alive. The last generation formed at $t_{\rm SFR} = 10.0$ Gyr is complete and the age of these stars ($A_{\rm s}$) is zero. Therefore:

$$A_{\rm s} = Age - t, \tag{5}$$

where t runs from 0.0 up to $t_{\rm SFH}$, which could be the same as *Age*, depending on the star formation model.

The final result at 10.0 Gyr is a mix of populations with different ages and metallicities formed with the star formation suggested by the chemical evolution model.

One of the problems in evolutionary synthesis codes are the oscillations in the evolution of spectral parameters in starburst models, because the post main sequence phases are not well sampled due to the faster evolution of stars after the hydrogen burning phase. As shown in Sect. 2, the problem is solved by interpolating in phases (evolutionary points) over the post hydrogen burning evolution, and interpolating in time and mass over the main sequence phases. Important points over the tracks are: the turn off (14), the base of RGB (23), and the tip of RGB (54).

To calculate which stars are alive at $A_{\rm s}$ in the post-main sequence region, the code first calculates the masses of stars at each evolutionary point since the turn off point up to EAGB (71) using the relations $t_{\rm a}(Z, m_{\rm i}, j)$ versus $m_{\rm i}$ on the tracks as shown in Fig. 5 (where $t_{\rm a}$ is the age of each evolutionary point j over each track and initial mass $m_{\rm i}$).

The $A_{\rm s}$ intersects the curves in Fig. 5 corresponding to one value for the mass at the turn-off ($m_{\rm i_{14}}(Z)$) and another one on the EAGB ($m_{\rm i_{84}}(Z)$). The values are obtained interpolating the two points adjacent to the intersection. This process is repeated for all 71 evolutionary stages beyond the ZAMS.

To sample those masses in main and pre-main sequence phases, we divide the mass range $m_{\rm l} \leq m_{\rm i} \leq m_{\rm i_{14}}$ into 80 to get a total of 151 masses for the synthetic population for each time step of evolution with age $A_{\rm s}$ at the required metallicity.

Finally, to obtain the stellar properties ($m_{\rm c}$, $L/L_{\odot}$, and $T_{\rm eff}$) of these 151 masses of the new synthetic population, the code has identified their four adjacent points ($V(Z_0, m_{\rm i_0})$, $V(Z_0, m_{\rm i_1})$, $V(Z_1, m_{\rm i_0})$, and $V(Z_1, m_{\rm i_1})$) over the tracks to interpolate every stellar variable in mass and metallicity, respectively. In the case of a population stars yet in post-MS stages, the code is able to apply the grid of 151 masses to stars on the main and pre-main sequence.

3.2. Transformation from theoretical to the observational plane

The stellar parameters in the synthetic population were transformed to the observable parameters by using the calibrations of Lejeune et al. (1997) and Lejeune et al. (1998), which include low resolution spectral energy distributions (SEDs) and broad band colors. Table 4 shows the grid of parameters covered by this library.

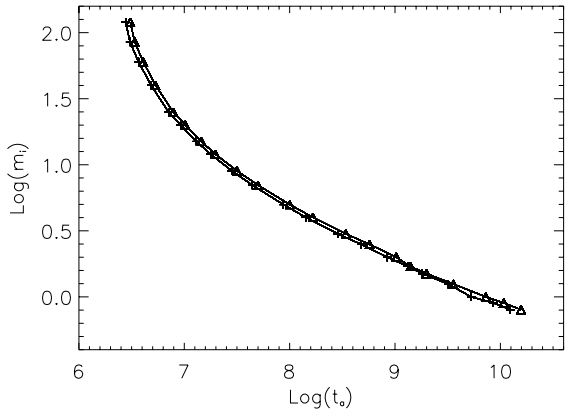

Fig. 5. Relations of evolutionary time $t_{\rm a}(Z, m_{\rm i}, j)$ versus initial mass $m_{\rm i}$ for the turn-off (crosses), and the EAGB (triangles) at $Z = Z_{\odot}$.

Table 4. Features of SEDs and broad band colors calibrations used in this work.

Parameters	Lejeune et al. (1997, 1998)
$T_{\rm eff}$ (K)	(2000, 50 000) K
$\log(g)$	(−1.02, 5.5)
$[M/H]$	(−5.0, 1.0)
$\lambda\lambda$ (nm)	(9.1, 160 000)
$n(\Delta\lambda)$	1221
Colors	14

Following the same procedure as in the tracks, we linearly interpolated or extrapolated (e.g. for the temperatures of the hottest stars) colors, indices, and spectra over this grid using the equations described in Sect. 2, but now for $[M/H]$, $T_{\rm eff}$, and $\log(g)$ (gravity), where $[M/H] = \log(Z/Z_{\odot})$, with $Z_{\odot} = 0.02$. Besides the spectrum and the broad band colors, we have included the Lick indices of Worthey et al. (1994) using the routine developed in González (1993).

We have to transform those variables given in magnitudes, like colors and indices, into luminosities or fluxes to integrate the observable variables for all stars alive.

The spectral variables are weighted by the numbers of stars and the average values are:

$$< L_f > = \frac{\int_0^{Age} \int_{m_l}^{m(t)} L_f(Z, m', t')\, w(m', t')\, {\rm d}m'\, {\rm d}t'}{\int_0^{Age} \int_{m_l}^{m(t)} w(m', t')\, {\rm d}m'\, {\rm d}t'}, \tag{6}$$

where the weights to obtain the average are defined

$$w(m', t') = \begin{cases} n(m', t') \times F_{\rm C} & \text{for indices} \\ n(m', t') \times L_{\rm bol} & \text{for colors} \\ n(m', t') & \text{for spectra.} \end{cases} \tag{7}$$

$F_{\rm C}$ is the continuum flux in the center of the index as defined by González (1993), $L_f(Z, m', t')$ is the stellar variable to integrate, $L_{\rm bol}$ is the bolometric luminosity, and $m(t)$ is the maximum mass of stars alive at time t.

Finally, integrated variables are obtained by using:

$$< (f_1 - f_0) > = -2.5 \times \log\left(\frac{< L_{f_1} >}{< L_{f_0} >}\right), \quad (8)$$

for indices and colors, and

$$< \mathrm{mag}_f > = -2.5 \times \log(< L_f >), \quad (9)$$

in the case of magnitude indices.

4. Evolution models

4.1. Tests for the evolutionary synthesis code

We have used instantaneous starburst models to test and compare our code with others commonly used.

In the first part, we test colors and spectral indices; in the second part spectra for young and old populations.

4.1.1. Colors and spectral indices

For the first part we assume the following set of conditions:

$\Phi(m_\mathrm{i}) \propto m^\alpha$, with $\alpha = -2.35$, lower mass limit $m_\mathrm{l} = 0.1$, and upper mass limit $m_\mathrm{h} = 100.0$; for SPECTRAL, we use the Geneva tracks with normal mass-loss rates.

1) In the first model we compare the evolution of colors at $Z = Z_\odot$ with those obtained from PEGASE97 (Fioc & Rocca-Volmerange 1997, FR) and GISSEL96 (Bruzual & Charlot 1993, BC). Figure 6 shows this comparison.

We can see from Fig. 6, that there is a good agreement between the three models for colors. The differences are due to the use of different spectral library (PEGASE97), or different stellar tracks (GISSEL96). In this figure it is possible to see a peak in the $(V - K)$ color of the FR model, around $\log(Age[\mathrm{Gyr}]) = -1.0$. It is produced by thermal pulses generated by stars in the range $(5.0 \leq m_\mathrm{i}/M_\odot \leq 10.0)$ at the tip of AGB, as explained by FR. The TP-AGB phase is not present in the Geneva tracks. Although this phase is present in the models of BC for low and intermediate mass, the BC and FR models do not agree, as we can see in Fig. 6. For a young population (around $\log(Age[\mathrm{Gyr}]) = -2.0$) we find agreement between colors from our model and those from FR. Alternatively, the agreement of the colors from our and the BC models is found for old populations (around $\log(Age[\mathrm{Gyr}]) = 1.0$).

2) In the second model we compare the same colors shown in Fig. 6 for different metallicities with those obtained from GISSEL96 (Fig. 7). Similarly, we compare the evolution of two Lick indices H_β and Mg_b in Fig. 8.

In Fig. 7a we compare models for the lowest metallicity reached by our code with models at the lowest metallicity in the Padova tracks used by GISSEL96. There is good agreement between models for different metallicities, except for the case of $Z = 0.0005$ where our code extrapolates.

As for the indices, both codes uses the Lick fitting functions. Our models predict a flat and constant evolution for young populations (around $\log(Age[\mathrm{Gyr}]) \leq -1.0$), while the indices from BC show variations. The differences are due to a different extrapolation scheme in BC. They extrapolate the fitting functions linearly to high temperatures (depending on

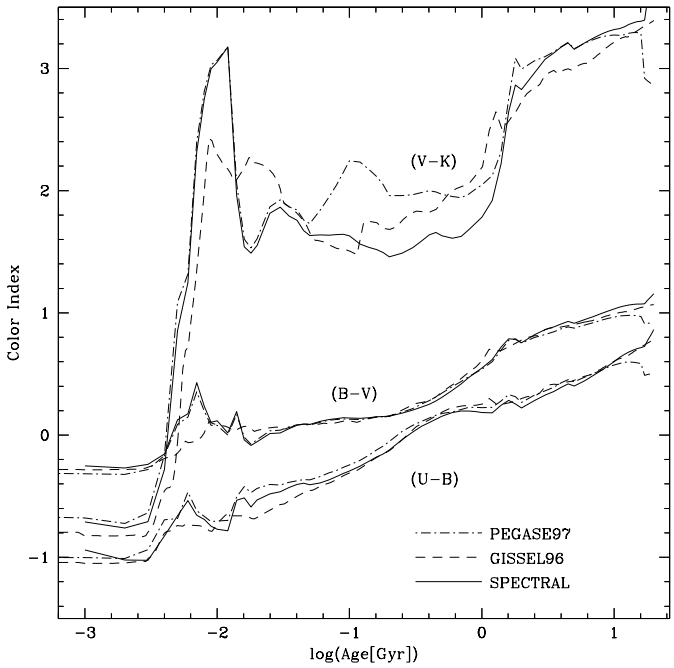

Fig. 6. Predicted color index evolution of a starburst at $Z_\odot$ by three different codes; PEGASE97, GISSEL96, and SPECTRAL.

T_eff, $\log(M/H)$, and $\log(g)$), which predict the value of each index, and we use the original fitting functions with a temperature limit around 13 000 K. There is agreement between both models for populations in the range of $\log(Age[\mathrm{Gyr}]) > -1.0$.

The spectral indices are quite sensitive to gravity and temperature: the presence of the TP-AGB in the models from BC produces considerable differences in the value of indices with respect to the SPECTRAL models for old stellar populations.

4.1.2. Spectra

We have performed test calculations for spectra in a different way. We have divided the test into two ranges, for young stellar populations and for old stellar populations. Both ranges were subdivided into three metallicities. We use instantaneous starbursts for the comparison.

For young populations we assume the following set of conditions:

$\Phi(m_\mathrm{i}) \propto m^\alpha$, with $\alpha = -2.35$, lower mass limit $m_\mathrm{l} = 1.0$, and upper mass limit $m_\mathrm{h} = 100.0$; for SPECTRAL we use the Geneva tracks with the high mass-loss rates.

1) In the first model we compare our spectra with different ages in the range of $10^{-3} \leq t/\mathrm{Gyr} \leq 0.9$ at $Z = Z_\odot$ with spectra produced by STARBURST99 (Leitherer et al. 1999). Figure 9 shows both set of spectra normalized to a population of 1 $M_\odot$. All models from STARBURST99 used here are without nebular emission.

There is very good agreement, as expected, because both codes use the same spectral library and the same stellar tracks. There is an additional spectral component in STARBURST99 in the UV part for ages between 3 and 5 Myr due to the WR phases. These features are not seen in our spectra because the models for massive stars with strong stellar winds are

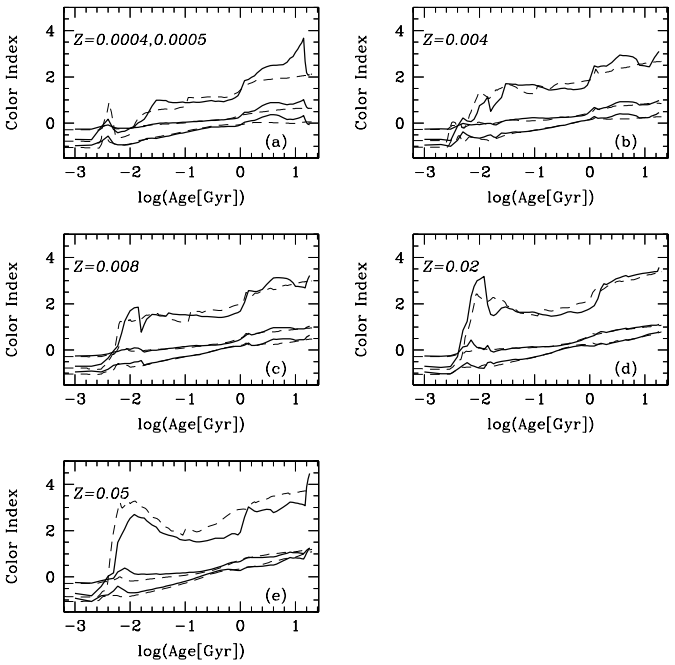

Fig. 7. Same as Fig. 6 but showing the color evolution of starbursts at different metallicities obtained with GISSEL96 (dashed lines) and SPECTRAL (full lines).

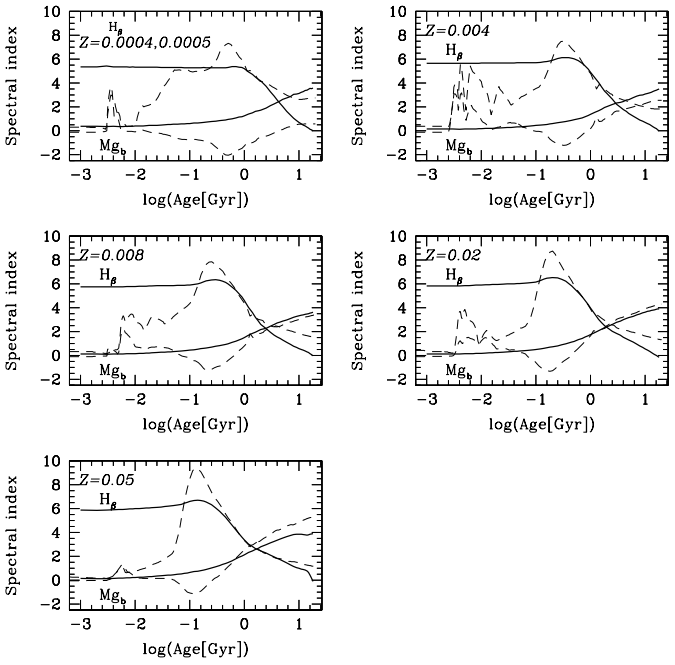

Fig. 8. Same as Fig. 6 but showing the spectral indices evolution of starbursts at different metallicities. GISSEL96 (dashed lines), and SPECTRAL (full lines).

not considered in our spectra library. This increase of luminosity in UV part appears in the STARBURST99 models at high metallicity, but not at low metallicity.

The differences are highlighted when we plot the $\log(L_{S99}/L_{SPECTRAL})$. Figure 10 shows the quantitative differences taking the $\log(L_{S99_k}/L_{S_k}) + 0.5k$ ($k = 0, 12$), where L_{S99} is the luminosity from STARBURST99's spectra and L_S from SPECTRAL.

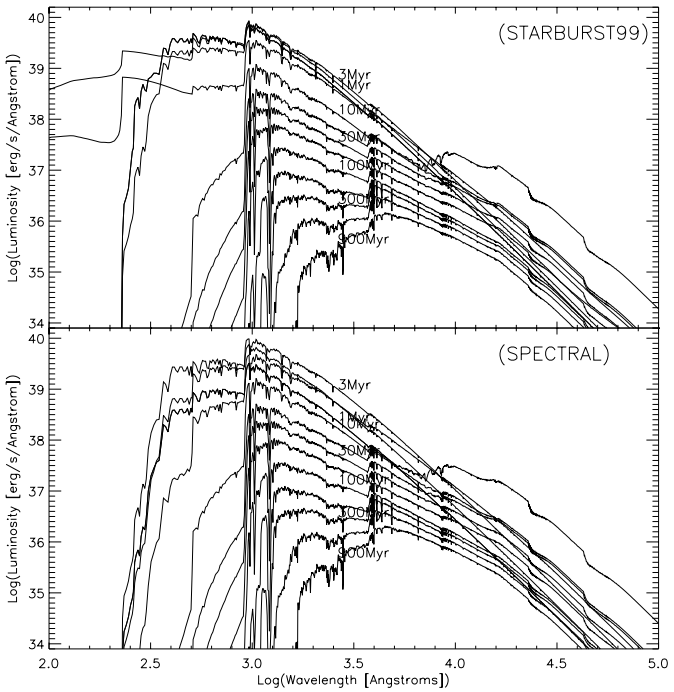

Fig. 9. Spectra from STARBURST99 and SPECTRAL at different ages, for a starburst at $Z = Z_\odot$.

We confirm the higher UV luminosity in the models of STARBURST99, and the decrease at lower metallicities of this feature. The artifacts around $Lyman_\alpha$ are produced by the different numerical methods used.

The same agreement with the models of Leitherer et al. (1999) is present in the other metallicities of the Geneva tracks as well, as shown in Vázquez (2001).

For old populations we assume the following set of conditions:

$\Phi(m_i) \propto m^\alpha$, with $\alpha = -2.35$, lower mass limit $m_l = 0.1$, and upper mass limit $m_h = 100.0$; for SPECTRAL we use the Geneva tracks with normal mass-loss rates.

2) In the first model we compare our spectra with different ages in the range $1.0 \leq t/\mathrm{Gyr} \leq 20.0$ at $Z = Z_\odot$ with spectra produced by GISSEL96 (BC). Figure 11 shows both sets of spectra normalized to a population of 1 $M_\odot$.

It is easy to see differences in Fig. 11 which are due to the stellar tracks used for each code, Padova (GISSEL96) and Geneva (SPECTRAL), respectively. The considered spectral library is the same, but not the same version, which is another source of differences. The main differences are in the blue part of the spectra, where we find a contribution in UV due to old stars in phases like HB and planetary nebulae predicted by an additional stellar library used by GISSEL96. These phases have no counterparts in our models.

Again, the $\log(L_{G96}/L_S)$ is higher for the models from GISSEL96. Figure 12 shows quantitative differences taking the $\log(L_{G96_k}/L_{S_k}) + k$ ($k = 0, 5$), where L_{G96} is the luminosity from GISSEL96's spectra and L_S from SPECTRAL.

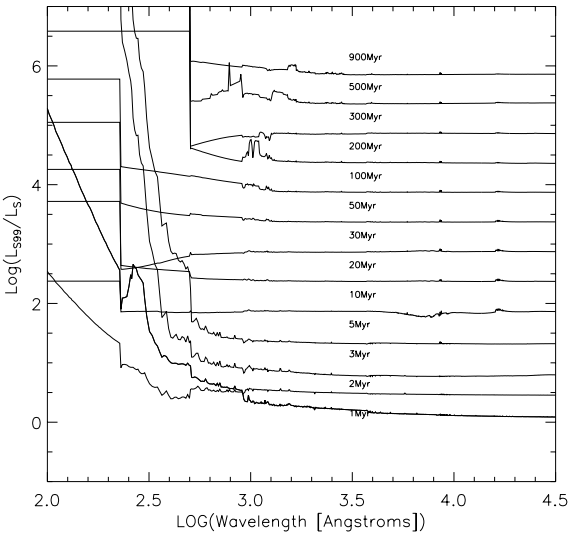

Fig. 10. Quantitative differences between our spectra and those from STARBURST99 at different ages, for a starburst at $Z = Z_{\odot}$.

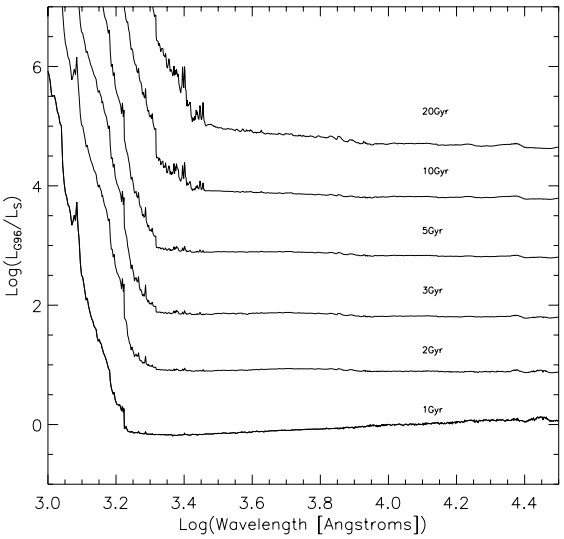

Fig. 12. Quantitative differences between our spectra and those from GISSEL96 at different ages, for a starburst at $Z = Z_{\odot}$.

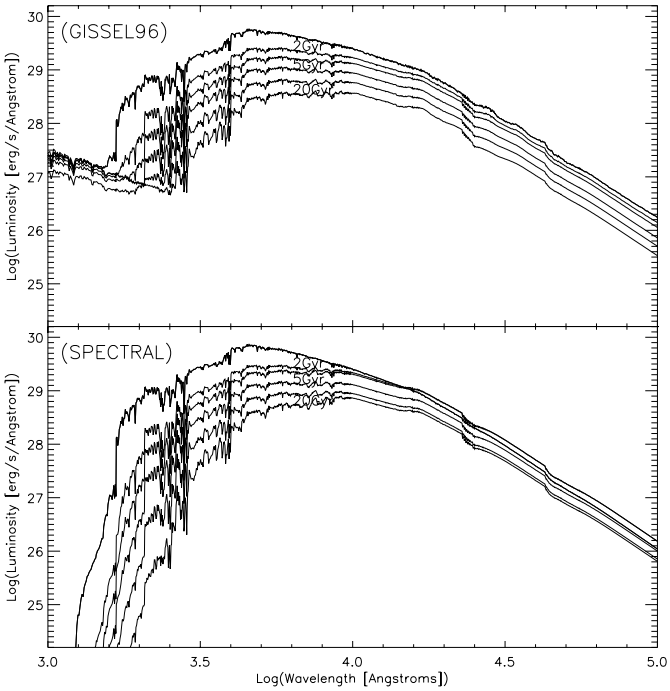

Fig. 11. Spectra from GISSEL96 and SPECTRAL at different ages, for a starburst at $Z = Z_{\odot}$.

The rest of models at different metallicities are shown in Vázquez (2001).

5. Models for the irregular Galaxy NGC 1560

Carigi et al. (1999) discussed the chemical evolution of three irregular galaxies: NGC 1560, II Zw 33 and a mean irregular galaxy. In attempting to apply spectro-chemical evolution models to these three galaxies, we searched for spectro-photometric measurements of these galaxies in the literature. In this work, we compute spectro-chemical evolution models only to NGC 1560 because: i) the nonbaryonic dark matter inside the Holmerg Radius is known for NGC 1560 and II Zw 33, which constrains the baryonic mass in the chemical evolution models. ii) Only NGC 1560, but neither II Zw 33, nor the sample of galaxies to calculate the mean irregular galaxy have photometric measurements to constrain the spectral models.

We have used three closed box models from Carigi et al. (1999) for NGC 1560 assuming a star formation rate proportional to the gas content and updated with yields from Maeder (1992) and van den Hoek & Groenewegen (1997) to be consistent with the stellar evolution models with the normal mass-loss rates used by our spectral code. These three chemical evolution models reproduce two constraints: the O/H abundance (Richer & McCall 1995) and $\mu = M_{\rm gas}/M_{\rm bar}$ (Walter et al. 1997; Broelis 1992), where $M_{\rm bar}$ is the mass of the baryonic matter. As shown in Fig. 13, all three models with different star formation rates do match the oxygen abundance in HII regions and $M_{\rm gas}$ observed in NGC 1560, however at different ages. Colors of this galaxy may constrain the age if we use evolutionary synthesis.

These models use the basic form for the IMF in the range of $0.01 \leq m_{\rm i}/M_{\odot} \leq 120.0$ as parameterized by Kroupa et al. (1993):

$$\Phi(m_{\rm i}) \sim \begin{cases} m_{\rm i}^{-\alpha} & \text{if } 0.01 \leq m_{\rm i}/M_{\odot} < 0.5, \\ m_{\rm i}^{-2.2} & \text{if } 0.5 \leq m_{\rm i}/M_{\odot} < 1.0, \\ m_{\rm i}^{-2.7} & \text{if } 1.0 \leq m_{\rm i}/M_{\odot} < 120.0 \end{cases} \quad (10)$$

where α depends on chemical constraints and age of the model, and has a different value for each model:

$$\alpha = \begin{cases} 2.21 & \text{0.1 Gyr Model} \\ 2.24 & \text{1.0 Gyr Model} \\ 2.27 & \text{10.0 Gyr Model} \end{cases} \quad (11)$$

α has to increase for models with older ages because NGC 1560 have had lower star formation rate during a longer time (to reproduce $M_{\rm gas}$) and a lower rate of SN (to reproduce the O abundance). Since the normalization of the IMF must be kept, the number of substellar objects ($m < 0.1\ M_{\odot}$) is higher, in models with older ages.

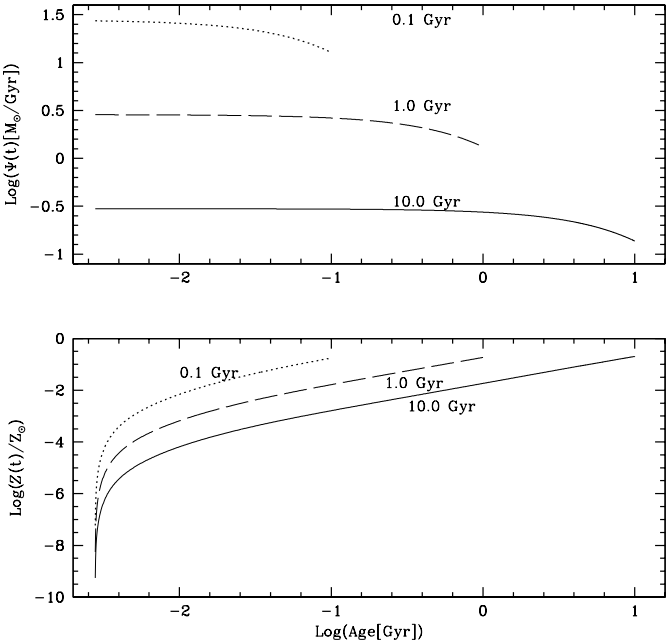

Fig. 13. Star formation rate and metallicity evolution for the three models at 0.1 Gyr (dotted line), 1.0 Gyr (dashed line), and 10.0 Gyr (continuous line).

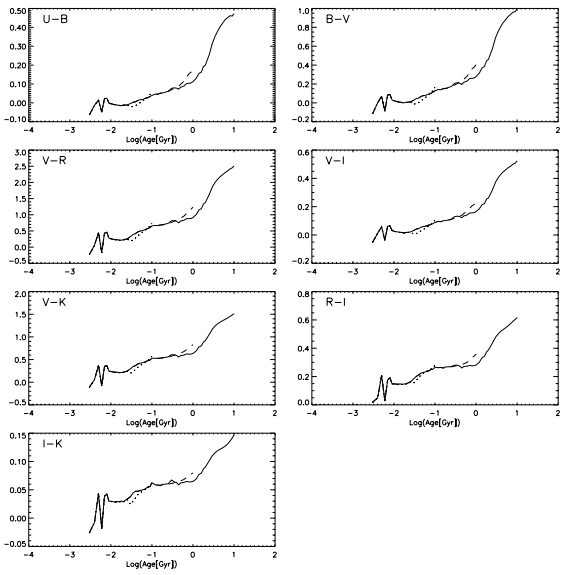

Fig. 14. Broad band colors evolution for the three models at 0.1 Gyr (dotted line), 1.0 Gyr (dashed line), and 10.0 Gyr (continuous line).

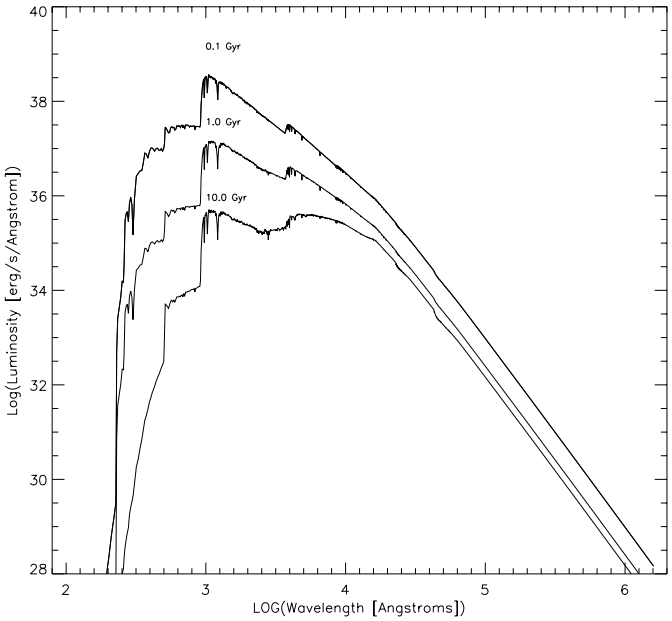

Fig. 15. The spectra produced for the three models.

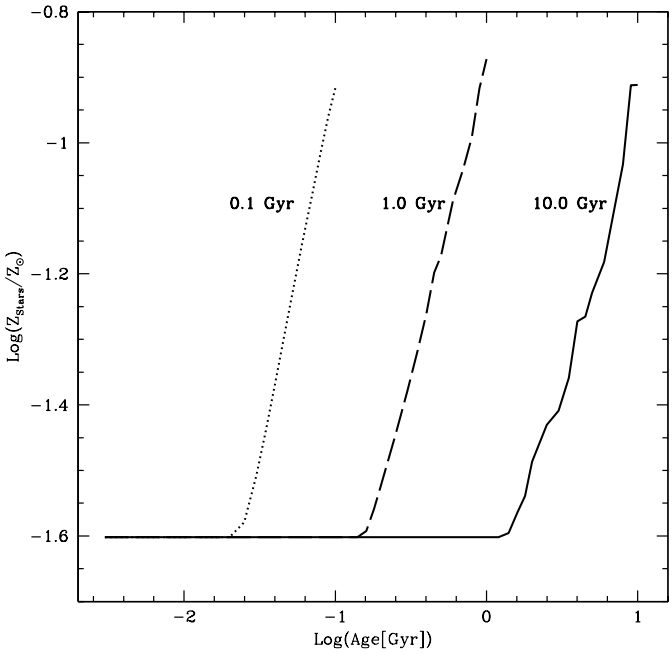

Fig. 16. Evolution of the luminosity-weighted stellar metallicity for three spectro-chemical evolution models.

We use $\Phi(m_{\rm i})$, $\Psi(t)$, and $Z(t)$ from the chemical models in SPECTRAL to produce three spectro-chemical evolution models. Figure 14 shows the evolution of some broad band colors predicted for this galaxy.

The rest of broad band colors and Lick indices for this set of models are shown in Vázquez (2001). The spectra for the spectro-chemical evolution models are shown in Fig. 15.

SPECTRAL permits one to follow the metallicity for stars weighted by light using their Eq. (10) with $L_{\rm bol}$. Figure 16 illustrates how SPECTRAL can follow the star formation and chemical enrichment histories. The luminosity-weighted metallicities for stars at $t_{\rm SFH}$ are $Z_{\rm stars}/Z_{\rm sun}$ = 0.12, 0.135, and 0.125 for models with ages of 0.1, 1.0, and 10.0 Gyr, respectively.

The main goal in this work is to compare our predictions for this galaxy with those obtained observationally. For this galaxy we have obtained $(U-B)_0$ and $(B-V)_0$ from the de Vaucouleurs RC3, which are mean values. The evolution and the comparison are reproduced in Fig. 17.

Figure 17 suggest that the model with an age of 10.0 Gyr fits the observations best. In contrast, the younger models disagree with the observations.

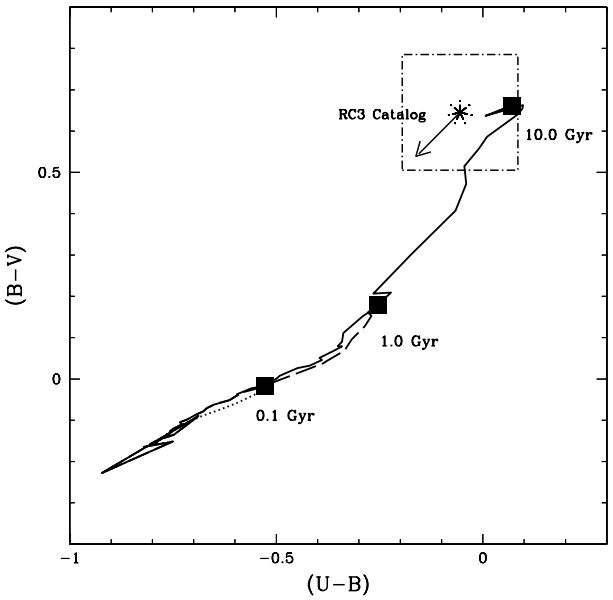

Fig. 17. Evolution of $(U-B)$ vs. $(B-V)$ for the three models in comparison with the observed values. Dotted line shows the 0.1 Gyr model, dashed line the 1.0 Gyr model, and continuous line the 10.0 Gyr model. The box shows the error for the values from the literature. The arrow indicates the reddening trend.

6. Conclusions

We have extended the tracks from the Geneva group, producing two new sets of tracks, one with high mass-loss rates for masses in the range of $12.0 \leq m_{\rm i}/M_{\odot} \leq 120.0$ and the other with normal mass-loss rates in the range of $0.08 \leq m_{\rm i}/M_{\odot} \leq 120.0$. These sets of tracks are complete and consistent for metallicities in the range of $0.001 \leq Z \leq 0.04$, they cover the phases from the main sequence up to the early asymptotic giant branch in the range $0.8 \leq m_{\rm i}/M_{\odot} \leq 120.0$ (except for stars in the range of [2.0,10.0] $M_{\odot}$, for which no AGB phase is included), and pre-main sequence and main sequence for masses in $0.08 \leq m_{\rm i}/M_{\odot} \leq 0.8$. Together with the spectral library, the code SPECTRAL is able to predict the spectral properties from stellar populations under a wide variety of conditions.

With this code, it is possible to build synthetic populations with sophisticated chemical evolution models, as long as the metallicity is in the range of $0.001 \leq Z \leq 0.04$.

The results for starburst evolution in broad band colors, spectral indices and spectra from our code agree very well with the same results obtained with other codes. SPECTRAL can be used in young stellar populations like in starburst or blue galaxies, or stellar populations inside cores of AGN's. In the same way, the code can be used for stellar populations in early type, spirals, or late-type galaxies.

In applying the chemical evolution models only, using observational constraints in Carigi et al. (1999) to NGC 1560, we find that it is not easy to constrain the age of the population. However, with the observed colors for this galaxy, a spectro-chemical evolution model can be fitted and a stellar population with an age around 10 Gyr and a luminosity-weighted metallicity $< Z > = 0.002$ of the stars are predicted.

We have obtained success in reproducing the values for simple star formation scenarios, and finally, we have matched very closely the values observed for two broad band colors in NGC 1560.

The code and stellar data base can be obtained under request or in `http://www.stsci.edu/~vazquez`

Acknowledgements. This work is part of the PhD thesis developed by Gerardo A. Vázquez in the IA-UNAM. We thank Gustavo Bruzual who made an extensive review of the code. Gerardo is similarly indebted to Gloria Koenigsberger for support during the final stages of his Ph.D. We thank the Instituto de Astronomía UNAM for financial support of Gerardo with a fellowship, resources and travel founds obtained through the projects PAPIIT, IN126098 and IN109696. We thank Gloria Koenigsberger, Luc Binette and Claus Leitherer for reading the manuscript. Thanks to Uta Fritze-v.Alvensleben to improve the manuscript and content of this article.

References

Arimoto, N., & Yoshii, Y. 1986, A&A, 164, 260
Broelis, A. 1992, A&A, 256, 19
Bruzual, G., & Charlot, S. 1993, ApJ, 405, 538 (BC)
Carigi, L., Colín, P., & Peimbert, M. 1999, ApJ, 514, 787
Chabrier, G., & Baraffe, I. 1997, A&A, 327, 1039 (CB)
Charbonnel, C., Meynet, G., Maeder, A., Schaller, G., & Schaerer, D. 1993, A&AS, 101, 415 (III)
Charbonnel, C., Meynet, G., Maeder, A., & Schaerer, D. 1996, A&AS, 115, 339 (VI)
Charbonnel, C., Däpen, W., Schaerer, D., et al. 1999, A&AS, 135, 405 (VIII)
de Vaucouleurs, G., de Vaucouleurs, A., Corwin, H. G., et al. 1991, Third Reference Catalog of Bright Galaxies (New York: Springer)
Einsel, C., Fritze-v.Alvensleben, U., Krueger, H., & Fricke, K. J. 1995, A&A, 296, 347
Fioc, M., & Rocca-Volmerange, B. 1997, 326, 950 (FR)
González, J. J. 1993, Ph.D. Thesis, University of California, Sta. Cruz
Kroupa, P., Tout, C. A., & Gilmore, G. 1993, MNRAS, 262, 545
Leitherer, C., Schaerer, D., Goldader, J. D., et al. 1999, ApJS, 123, 3
Lejeune, T., Cuisinier, F., & Buser, R. 1997, A&AS, 125, 229
Lejeune, T., Cuisinier, F., & Buser, R. 1998, A&AS, 130, 65
Lindner, U., Fritze-v.Alvensleben, U., & Fricke, K. J. 1999, A&A, 341, 709
Maeder, G. 1992, A&A, 264, 105
Moeller, C. S., Fritze-v.Alvensleben, U., & Fricke, K. J. 1997, A&A, 317, 676
Meynet, G., Maeder, G., Schaller, D., Schaerer, D., & Charbonnel, C. 1994, A&AS, 103, 97 (V)
Mowlavi, N., Schaerer, D., Meynet, G., et al. 1998, A&AS, 128, 471 (VII)
Richer, M., & McCall, M. 1995, ApJ, 445, 659
Schaerer, D., Meynet, G., Maeder, A., & Schaller, G. 1993a, A&AS, 98, 523 (II)
Schaerer, D., Charbonnel, C., Meynet, G., Maeder, A., & Schaller, G. 1993b, A&AS, 102, 339 (IV)
Schaller, G., Schaerer, D., Meynet, G., & Maeder, A. 1992, A&AS, 96, 269 (I)
Tinsley, B. 1972, A&A, 20, 383
van den Hoek, & Groenewegen 1997, A&AS, 123, 305
Vazdekis, A., Casuso, E., Peletier, R. F., & Beckman, J. E. 1996, ApJS, 106, 307
Vázquez, G. A. 2001, Ph.D. Thesis, Instituto de Astronomía, UNAM
Walter, F., Brinks, E., Duric, N., & Klein, U. 1997, AJ, 113, 2031
Worthey, G., Faber, S. M., González, J. J., & Burstein, D. 1994, ApJS, 94, 687